THE ASTROPHYSICAL JOURNAL, 418:414–425, 1993 November 20

THE PRE–MAIN-SEQUENCE EVOLUTION OF INTERMEDIATE-MASS STARS

FRANCESCO PALLA
Osservatorio Astrofisico di Arcetri, Largo E. Fermi, 5, 50125 Firenze, Italy
AND
STEVEN W. STAHLER
Astronomy Department, University of California, Berkeley, Berkeley, CA 94720; and NASA/Ames Research Center
Received 1993 March 11; accepted 1993 May 24

ABSTRACT

We calculate numerically the structure and evolution of pre–main-sequence stars with masses from 1 to 6 $M_\odot$. These stars are assumed to originate from protostars accreting within molecular clouds. For masses from 2 to 4 $M_\odot$, the stellar luminosity first increases markedly during a protracted epoch of nonhomologous contraction and thermal relaxation. Deuterium burns in a subsurface shell throughout this period. More massive objects are thermally relaxed from the start; they contract homologously, with fully radiative interiors. Stars with masses greater then 8 $M_\odot$ have no pre–main-sequence phase, since they are already burning hydrogen by the time protostellar accretion has ended. We summarize our results by presenting a new set of evolutionary tracks in the H-R diagram.

Our calculations imply that Herbig Ae and Be stars are substantially younger than previously believed. The upper boundary to their distribution in the H-R diagram is well matched by our theoretical birthline. The presence in these stars of emission lines and strong winds is *not* linked to an outer convection zone, since our models show that such convection always vanishes with rising effective temperature. Finally, while residual accretion from circumstellar disks may be occurring, we argue that the associated mass transfer rates are not high enough to account for the stars' observed infrared excesses.

Subject headings: stars: evolution — stars: interiors — stars: pre–main-sequence

1. INTRODUCTION

Over three decades ago, Herbig (1960) conducted a successful search for young stars more massive than the solar-type T Tauri stars but still contracting toward the main sequence. Although these Herbig Ae and Be stars are rare in comparison with their low-mass counterparts, their higher luminosities make them attractive objects for observational study. In the years since their discovery, their pre–main-sequence nature has been amply confirmed. Strom et al. (1972) used surface gravity measurements to show that the radii of selected stars were indeed larger than main-sequence values, while Finkenzeller & Jankovics (1984) employed radial velocities to verify the stars' kinematic link to nearby molecular cloud gas. Finkenzeller & Mundt (1984) cataloged the properties of 57 Ae and Be stars and found spectroscopic evidence for strong winds from a substantial fraction. More recently, attention has turned to the large continuum excesses at infrared and longer wavelengths, in the hope that these could provide evidence for residual accretion of circumstellar matter (Hillenbrand et al. 1992; Lada & Adams 1992; Natta et al. 1992).

From a theoretical perspective, the study of more massive young stars offers a new opportunity to test, and therefore to modify, our conception of early stellar evolution. In the classic studies of Henyey, LeLevier, & Levee (1955) and Hayashi (1961), it was established that pre–main-sequence stars of all masses derive their luminosity primarily by gravitational contraction through a sequence of quasi-static configurations. The calculations assumed that stars begin this contraction as fully convective objects, with radii nearly two orders of magnitude larger than their final, ZAMS values (Iben 1965; Ezer & Cameron 1967). However, such large radii could not have been attained during the previous protostar phase, when the stars were gathering mass from their parent interstellar clouds (Larson 1969; Winkler & Newman 1980; Stahler, Shu, & Taam 1980). By combining a protostar mass-radius relation with standard pre–main-sequence theory, Stahler (1983) showed that the evolutionary tracks of low-mass stars should begin from a well-defined "birthline" in the H-R diagram. This prediction is in accord with the observations of T Tauri stars (Cohen & Kuhi 1979; Stahler 1988).

In the case of intermediate-mass stars, the modification of initial conditions has an even greater impact. For plausible accretion rates during the protostar phase, stars more massive than about 2 $M_\odot$ are radiatively stable when they begin their quasi-static contraction. Any anomalies in such a star's internal thermal state can die away only through the relatively slow process of photon diffusion. In other words, the imprint of the prior accretion history persists much longer than in the low-mass, convective case. One result is that the star's surface luminosity can be expected to rise sharply early during contraction (Stahler 1989). Another is that the star inherits a thick, subsurface mantle of deuterium (Palla & Stahler 1991); this deuterium must ignite in a shell and fuse to helium during the subsequent approach to the ZAMS.

Our present purpose, then, is to reexamine the pre–main-sequence evolution of stars more massive than 1 $M_\odot$, employing initial conditions that could plausibly have been attained during the protostar phase. We take these conditions from our own recently completed study of intermediate-mass protostars (Palla & Stahler 1990, 1991, 1992). We have already adduced several key implications for pre–main-sequence evolution on the basis of this work. First, the use of our derived protostar mass-radius relation yields a birthline that indeed matches the upper envelope to the distribution of Ae and Be stars in the

H-R diagram (Palla & Stahler 1990). Second, the modest initial radii implied by our calculation translate into a substantial reduction in contraction ages compared to traditional values. Such a large age reduction is *not* present for typical T Tauri stars of lower mass (Stahler 1983) but is in general agreement with the empirical evidence for vigorous surface activity in Ae and Be stars (Catala 1989). Finally, our calculations have set an upper mass limit to the pre–main-sequence phase itself. We have predicted that only stars less massive than about 8 $M_\odot$ can still be contracting toward the ZAMS, since heavier stars ignite ordinary hydrogen while still undergoing protostellar accretion.

In our previous study, we constructed a number of different model sequences of protostars, in order to gauge the effect of varying the properties of the accretion flow (Palla & Stahler 1992). The strategy pursued here is to choose one of these sequences and follow the evolution of selected models, in the mass range $1\ M_\odot \leq M_* \leq 8\ M_\odot$, from the birthline to the ZAMS. We find that, for a large fraction of stars in this range, the stellar interior is not thermally relaxed at the end of accretion, and the luminosity indeed rises with time. During this adjustment period, the star's surface layers actually expand as they absorb heat from the contracting interior. Concurrently, deuterium in these layers does ignite, as expected, and the burning shell gradually retreats to the stellar surface. However, the shell burning is too weak to maintain outer convection once the surface temperature climbs to 10^4 K. Thus, contrary to our own speculation (Palla & Stahler 1990), the observed surface activity of Ae and Be stars *cannot* be attributed to a dynamo-generated magnetic field (see also Tijn A Djie, Remijn, & Thé 1984).

In the next section, we motivate our choice of initial conditions, by drawing on the results of the protostar study. Section 3 describes our computational approach. The initial pre–main-sequence evolution of the stars and the thermal relaxation process are detailed in § 4, while the approach to the ZAMS is presented in § 5. We also indicate how our findings would be affected by modifications of the protostar phase. Finally, in § 6, we discuss the implications of this work for models of surface activity and infrared excess.

2. PROTOSTELLAR INITIAL CONDITIONS: A REVIEW

2.1. *Thermal Relaxation*

The structure and evolution of pre–main-sequence stars of low mass is dominated by the fact that they transport energy through thermal convection (Hayashi 1961). To see why, we recall that a star of mass M_* and radius R_* can carry radiatively an energy per unit time equal to

$$L_{\rm rad} = L_0 (M_*/M_\odot)^{11/2} (R_*/R_\odot)^{-1/2}\ , \qquad (1)$$

where the precise value of L_0, a luminosity of order 1 $L_\odot$, depends on the star's detailed structure (Cox & Giuli 1968). Equation (1) assumes that the star's interior opacity obeys Kramers's Law; this assumption is valid for the densities and temperatures of interest. The quantity $L_{\rm rad}$ is to be compared with $L_{\rm surf}$, the luminosity which the star of effective temperature $T_{\rm eff}$ can radiate into space:

$$L_{\rm surf} = 4\pi R_*^2 \sigma T_{\rm eff}^4\ . \qquad (2)$$

For low-mass stars, $L_{\rm surf}$ is larger than $L_{\rm rad}$, i.e., the rate of energy loss from the surface exceeds that which can be supplied from the inside by photon transport. Therefore, regardless of the star's thermal state prior to pre–main-sequence contraction, it quickly turns convectively unstable (e.g., von Sengbusch 1968). Convection carries the bulk of the interior energy, and the convective and radiative contributions, $L_{\rm con}$ and $L_{\rm rad}$, together sum to $L_{\rm surf}$.

The extreme mass sensitivity of $L_{\rm rad}$ implies that this quantity can exceed $L_{\rm surf}$ for modest stellar masses. Pre–main-sequence stars in this condition are essentially radiative objects, but they are *thermally unrelaxed* (Stahler 1989). The energy per unit time transported through the deep interior now *exceeds* that which the surface can radiate. A thick layer of gas beneath the surface heats up, and the surface luminosity increases with time until $L_{\rm surf}$ equals $L_{\rm rad}$. The heat supplied to the surface layers comes from the contracting deep interior. In contrast to the situation described in classical pre–main-sequence theory, the star may be said to undergo *nonhomologous* quasi-static contraction.

Underlying this discussion is our assumption that the star's initial surface temperature has a relatively low value like those characterizing solar-type pre–main-sequence stars. The value of $T_{\rm eff}$ will indeed be low as long as the interior distribution of specific entropy is simply that laid down by accretion during the prior protostar phase (Stahler 1989). Since it is precisely the entropy distribution which is altered during thermal relaxation, the star in question must not have had time to relax thermally while it was still gaining mass from its parent cloud. As a quantitative criterion, we may compare the Kelvin-Hemholtz time scale, $t_{\rm KH} \equiv GM_*^2/(R_* L_{\rm rad})$, with the accretion time, $t_{\rm acc} \equiv M_*/\dot{M}$. Here, $\dot{M}$, the protostellar mass accretion rate, is assumed to be independent of M_*, in accordance with current theory (Shu 1977). Equivalently, we compare $L_{\rm rad}$ with $L_{\rm acc}$, where $L_{\rm acc}$ is $GM_*\dot{M}/R_*$, the luminosity released by accretion onto the protostellar surface. The two inequalities, $L_{\rm rad} > L_{\rm surf}$ and $L_{\rm acc} > L_{\rm rad}$, must *both* be met if the star is to undergo nonhomologous contraction. It is clear, however, that the same strong increase of $L_{\rm rad}$ with mass which guaranteed the first inequality will eventually cause the second one to be violated, for sufficiently massive stars.

We thus arrive at the conclusion that the process of thermal relaxation, and the attendent rise in surface luminosity, occur only within a restricted mass interval. The situation is illustrated graphically in Figure 1, which shows the mass dependence of several luminosities for protostars accreting at 10^{-5} $M_\odot$ yr^{-1} (Palla & Stahler 1992). The luminosity $L_{\rm surf}$ is the actual surface value in each model; since the calculation employed photospheric boundary conditions, $L_{\rm surf}$ is also the pre–main-sequence luminosity just after the end of accretion. The quantity $L_{\rm rad}$ is the peak interior value of the radiative portion of the luminosity. The condition $L_{\rm surf} = L_{\rm rad}$ is met at the mass M_1, here equal to 2.4 $M_\odot$. At the mass M_3, which has the value 3.9 $M_\odot$, $L_{\rm acc}$ equals $L_{\rm rad}$. For pre–main-sequence stars with $M_* > M_3$, the surface temperature does *not* start out so low that $L_{\rm rad}$ exceeds $L_{\rm surf}$. Instead, the two luminosities are equal, and $T_{\rm eff}$ increases during the subsequent evolution to maintain this equality. The star contracts *homologously*, i.e., all interior mass shells lose heat. In the H-R diagram, the star follows a nearly horizontal path, as first described by Henyey et al. (1955).

It is apparent that the pre–main-sequence evolution of intermediate-mass stars is more closely tied to protostellar conditions than in the case of low-mass stars. Within the latter, thermal convection quickly homogenizes any interior entropy distribution. In more massive stars, the entropy can be

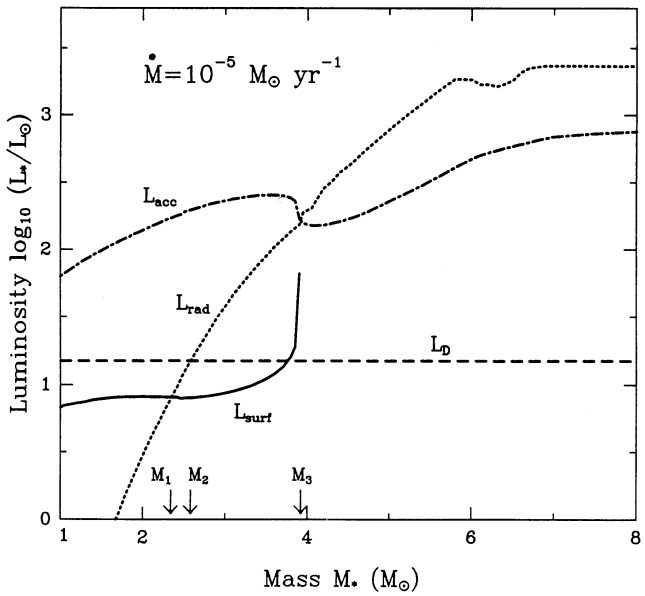

FIG. 1.—The mass dependence of luminosities in protostars accreting at 10^{-5} $M_\odot$ yr^{-1}; from Palla & Stahler (1992). Shown as a function of stellar mass are the accretion luminosity, L_{acc}; the luminosity carried by radiation, L_{rad}; the surface luminosity, L_{surf}; and the deuterium-generated value, L_D. The arrows on the horizontal axis mark the critical masses where L_{rad} intersects L_{surf}, L_D, and L_{acc}, respectively. At the last point L_{surf} climbs steeply to join L_{rad}, as shown.

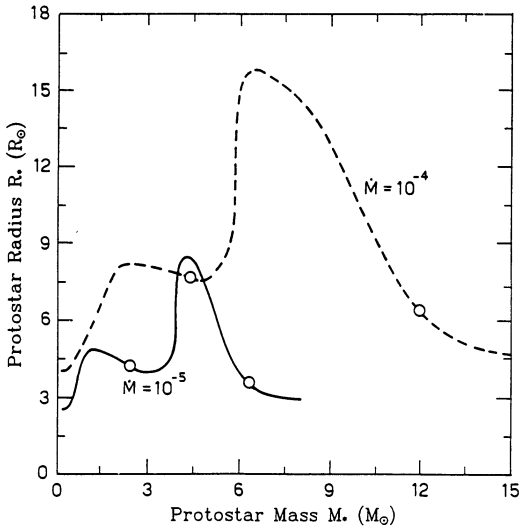

FIG. 2.—The protostar mass-radius relation; from Palla & Stahler (1992). The solid curve represents an evolutionary sequence computed with $\dot{M} = 10^{-5}$ $M_\odot$ yr^{-1}, while the dashed curve corresponds to $\dot{M} = 10^{-4}$ $M_\odot$ yr^{-1}. The two open circles on each curve mark, from left to right, the onset of deuterium shell burning and the central ignition of ordinary hydrogen.

altered, i.e., the star can thermally relax, only through the much slower process of radiative diffusion.[1] The existence of an upper mass limit to the relaxation phenomenon is evident in Figure 2, which reproduces the protostellar mass-radius relation from our earlier study (Palla & Stahler 1992). The two curves correspond to different assumed values of $\dot{M}$, as indicated. In each case, the protostellar radius $R_*(M_*)$, undergoes a very steep rise following the shell ignition of deuterium (*first open circle*). After reaching its maximum, $R_*(M_*)$ declines smoothly, until ordinary hydrogen ignites (*second open circle*). This final gravitational contraction is homologous. Thus, the pre–main-sequence stars descended from these most massive protostars complete their contraction as thermally relaxed objects.

Under the assumption that stars end their accretion phase relatively quickly, through the action of a powerful wind, the protostellar mass-radius relation gives directly the starting radii for pre–main-sequence contraction. In our previous study, we constructed models using both shock-type and photospheric outer boundary conditions, the latter intended to mimic crudely the effect of accretion through a circumstellar disk. The mass-radius relation computed with $\dot{M} = 10^{-5}$ $M_\odot$ yr^{-1}, and with either prescription for the boundary, yields a satisfactory birthline for the observed Herbig Ae and Be stars (Palla & Stahler 1992). Accordingly, we have adopted the sequence constructed with this value of $\dot{M}$ and photospheric boundary conditions to supply starting models for our pre–main-sequence calculations. As seen in Figure 2, protostars built up in this manner cease their contraction and reach the ZAMS by $M_* = 8$ $M_\odot$. This mass, then, provides a natural upper bound for the present calculation, since more massive stars are first optically visible when they are already on the main sequence.

[1] We are assuming that deuterium burning does not significantly alter the interior entropy; see § 4 below.

2.2. *Deuterium Mantle*

The fusion of deuterium to helium plays a dominant role in the evolution of low-mass protostars, but fades in significance for those of higher mass. Deuterium burning turns a star convectively unstable if L_D, the energy per unit time released by the fusion reaction, exceeds L_{rad}. For protostars more massive than a few tenths of a solar mass, deuterium burns as fast as it is being accreted from the parent cloud. Thus, L_D is given by

$$L_D = \dot{M}\delta\,, \tag{3}$$

where δ is the deuterium fusion energy per unit mass in the accreted interstellar gas. The mass at which L_D equals L_{rad} is denoted M_2 in Figure 1. In protostars with $M_* > M_2$, deuterium is unable to maintain convection throughout the entire star.

In our previous study, we followed in detail the disappearance of global convection. An interior mass shell, which we termed the *radiative barrier*, first becomes stable against convection. All deuterium within the barrier is quickly scoured out, leaving a depleted central core and a thick mantle of unburned fuel in the outer layers. Within this mantle, deuterium burns as a shell source; it is the ignition of the shell that creates the rapid swelling of the star seen in Figure 2. The burning maintains convection only in the outermost portion of the mantle (see Fig. 10 of Palla & Stahler 1991). Since these surface layers can supply fuel to the mantle in a steady state fashion, the deuterium-burning luminosity is still given by equation (3).

For a pre–main-sequence star of fixed mass M_*, the amount and distribution of deuterium is that which a protostar of the same mass acquired in the course of its accretion history. Figure 3 shows the development of the fractional deuterium concentration, f_D, in a protostar accreting at $\dot{M} = 10^{-5}$ $M_\odot$ yr^{-1}. Here, f_D is calculated relative to the interstellar concen-

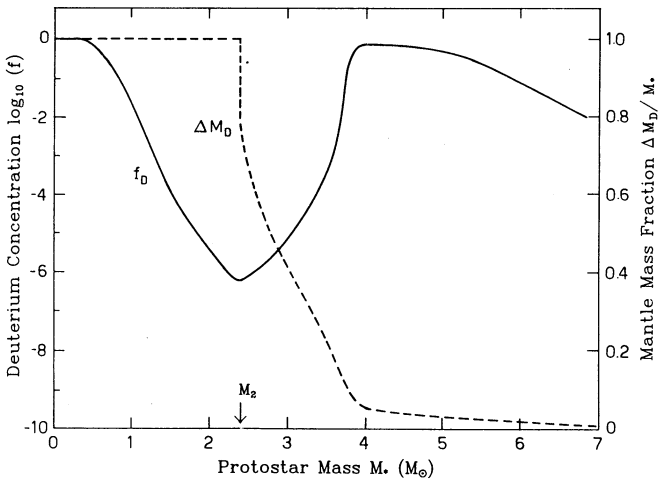

FIG. 3.—Evolution of deuterium in a protostar accreting at $10^{-5}\ M_\odot\ \mathrm{yr}^{-1}$; from Palla & Stahler (1992). Plotted as a function of stellar mass are f_D, the fractional deuterium concentration (*solid curve*) and ΔM_D, the mass of the deuterium mantle (*dashed curve*). Both curves show an abrupt change at $M_2 = 2.44\ M_\odot$, the mass where the radiative barrier first appears. After this time, f_D represents the average concentration only within the deuterium mantle.

tration, assuming a standard [D/H] value of 2.5×10^{-5} (Geiss & Reeves 1981). Shown also in the figure is ΔM_D, the mass at any time which has a nonzero deuterium abundance. The abrupt break in ΔM_D at $M_* = 2.44\ M_\odot$ marks the appearance of the radiative barrier and the rapid loss of the interior supply of deuterium.

Figure 3 shows that f_D declines quite rapidly for $M_* \geq 1\ M_\odot$, even though the star is fully convective, and therefore accreting deuterium as fast as it is being consumed. Actually, consumption slightly exceeds accretion, and L_D differs correspondingly from the value in equation (3). According to equation (50) of Stahler (1988), the evolution of f_D in a fully convective protostar is given by

$$M_* \frac{df_D}{dM_*} = 1 - f_D - \frac{L_D}{\dot{M}\delta}, \tag{4}$$

from which it follows that

$$L_D = \dot{M}\delta\left[1 - \frac{d(f_D M_*)}{dM_*}\right]. \tag{5}$$

Since the product $f_D M_*$ is proportional to the total deuterium content in a fully convective star, equation (5) shows that any net loss of deuterium implies that L_D exceeds $\dot{M}\delta$. Such loss is inevitable, because of the slowly rising interior temperature of the protostar. The local rate of deuterium energy generation per unit mass, $\epsilon_D(\rho, T)$, increases roughly as T^n, where $n \approx 12$ (Harris et al. 1983). Integration of ϵ_D over interior mass shells then yields another expression for L_D:

$$L_D = f_D[\mathrm{D/H}](L_D)_0\left(\frac{M_*}{M_\odot}\right)^{2+n}\left(\frac{R_*}{R_\odot}\right)^{-3-n}, \tag{6}$$

where $(L_D)_0 \equiv 1.9 \times 10^{17}\ L_\odot$. Equation (6) is taken from equation (49) of Stahler (1988), ignoring the effect of a surface hydrogen ionization layer. In our protostar calculations, we effectively used equation (6) to determine f_D at each time step, provisionally setting L_D equal to $\dot{M}\delta$. Numerical evaluation of the derivative in equation (5) then gave us the slight excess of L_D over this steady-state value.

The fall of f_D continues until the radiative barrier appears, i.e., when M_* equals M_2. Following the rapid burning interior to the barrier, deuterium exists only in the mantle. Although the outermost portion of the mantle is well mixed by convection, the radiative layers inside have a gradation of deuterium concentrations. The value of f_D shown in Figure 3 was obtained by mass-averaging the concentration within the mantle at each time step. The radiative-convective boundary starts at the inner edge of the mantle, but retreats to the surface by $M_* = 3.85\ M_\odot$, when the stellar radius swells sharply. For larger protostar masses, the mantle is almost entirely radiative, but is still consuming deuterium at its inner edge at the steady state rate of equation (3). As seen in Figure 3, the shrinking of the mantle actually leads to a temporary increase of f_D toward unity, followed by a slow decline for $M \gtrsim 4\ M_\odot$. The total deuterium content, as measured by $f_D \Delta M_D$, falls during the period of full convection, rises temporarily while the outer convection zone retreats, and thereafter continues to decline monotonically.

Our results concerning the protostar's supply of deuterium mark a departure from classical pre–main-sequence theory. Early on, Salpeter (1954) recognized that deuterium ignition could impede the gravitational contraction of a young star of fixed mass. Bodenheimer (1966) first included this effect in numerical calculations, and Grossman & Graboske (1971) showed how the burning could slow or even halt contraction temporarily over a range of masses. More recently, Mazzitelli & Moretti (1980) followed the process in solar-type pre–main-sequence stars, using an updated value of the interstellar [D/H]. All of these calculations ignored the protostar phase, and followed the traditional assumption that a pre–main-sequence star begins with such a large radius, and therefore low central temperature, that deuterium is not burned until the star contracts by a large amount. Such an energy-rich fuel is indeed available in the very low mass stars which are too cold to ignite it during accretion (Stahler et al. 1980). However, for the intermediate-mass stars of interest here, the deuterium supply is severely limited because of prior protostellar consumption, and the effect of this fuel on the subsequent contraction is correspondingly diminished.

3. METHOD OF SOLUTION

As in our protostar calculations, we take the star to be spherically symmetric, and neglect any influence of rotation or magnetic fields. We have calculated the evolution of stars with masses of 1.5, 2.0, 2.5, 3.0, 3.5, 4.0, 5.0, and 6.0 $M_\odot$. For each mass investigated, we took as the initial state the protostar model of the same mass from Palla & Stahler (1992), for the case $\dot{M} = 1 \times 10^{-5}\ \mathrm{yr}^{-1}$. That is, we have assumed that accretion onto the protostar from its parent cloud and circumstellar disk ends instantaneously. A more realistic assessment of the gradual falloff of accretion due to the action of a protostellar wind is beyond the scope of this study.

To follow the evolution of a given mass, we solved numerically the four stellar structure equations. The outer boundary conditions were the standard photospheric relations. The heat equation was solved implicitly, as described in § 2.2 of Palla & Stahler (1991), but without the mass accretion term. We again treated the calculation as a two-point boundary value problem, and employed a shooting-splitting technique in our numerical integrations (Firnett & Troesch 1974). A typical model required 350 spatial zones for sufficient integration accuracy. In convectively unstable regions, we used mixing-

length theory to relate the luminosity to the entropy gradient (Baker & Temesvary 1966), adopting a ratio of mixing length to pressure scale height of 1.5. The total number of time steps depended on the stellar mass, since, under our initial conditions, heavier stars begin their evolution much closer to the ZAMS. For $M_* = 2\ M_\odot$, 75 models were constructed, while for the largest mass considered, $M_* = 6\ M_\odot$, 20 models sufficed to cover the entire evolution.

The input physics adopted here, including the tabulation of Rosseland mean opacities and equation of state, as well as the choice of initial nuclear abundances, follows that in our protostar study. The total nuclear energy generation rate, $\epsilon(\rho, T)$, includes both the deuterium fusion reaction $^2\mathrm{H}(p, \gamma)^3\mathrm{He}$ (Harris et al. 1983) and the hydrogen-burning reactions in the *p-p* chain and CN cycle (Fowler, Caughlan, & Zimmerman 1975). Although interstellar lithium also ignites in the course of pre–main-sequence contraction (Bodenheimer 1965; D'Antona & Mazzitelli 1984), its relatively tiny abundance renders the effect energetically and structurally insignificant. A full account of the problem of pre–main-sequence lithium depletion can be found in D'Antona (1991). Mazzitelli (1989) has examined critically the influence of input physics on the construction of evolutionary tracks.

4. EARLY EVOLUTION

4.1. *Fully Convective Stars*

It is convenient to consider separately those stars which contract as fully convective objects from those with radiative interiors. As discussed in § 2.1 and shown in Figure 1, the division can be established through comparison of the two luminosities $L_{\rm surf}$ and $L_{\rm rad}$. Stars with $M_* < M_1$ are fully convective due to surface cooling as soon as they appear as optically visible objects. Now for $\dot{M} = 10^{-5}\ M_\odot\ \mathrm{yr}^{-1}$, the value of M_1 of 2.35 $M_\odot$ is coincidentally close to the mass, M_2, of 2.44 $M_\odot$ at which the radiative barrier first appears. The fact that $M_1 \approx M_2$ means that stars which were fully convective as protostars from deuterium burning remain so, at least for a time, following the end of accretion. The mass M_2 is significantly greater than M_1 in stars built up with higher accretion rates. We will discuss this case in § 5.2 below.

Figure 4 depicts, in the H-R diagram, the first 3×10^6 yr in the pre–main-sequence evolution of stars with masses of 1.5 and 2.0 $M_\odot$. Since both stars begin fully convective, they follow paths similar to those first calculated by Hayashi (1961). However, the initial radii are much smaller than envisioned in the classical theory, so that the convective phases are considerably shorter. In particular, the 2 $M_\odot$ star, with a mass close to the critical value M_1, contracts for only 1.1×10^4 yr before a radiative core appears at its center. The figure shows that the stellar radius actually swells during the spread of the radiative region. This swelling is a sign of nonhomologous contraction.

The nature of the contraction is further illustrated by the evolution of specific entropy, shown in Figure 5. Both stars begin with the uniform entropy distributions enforced by convective mixing. In both, too, there is a sharp drop in entropy near the surface, where hydrogen and helium are recombining (see § 4.1 of Stahler, Palla, & Salpeter 1986). The spreading of the radiative regions, in which the entropy increases outward, is also seen in both models.

As the stars radiate heat from their surfaces, their *average* interior entropy must drop. For $M_* = 1.5\ M_\odot$, the decline within the radiative core is much faster than that in the convective exterior. For the 2 $M_\odot$ star, in which the radiative region has spread farther, the exterior entropy actually increases. In both cases, a portion of the heat lost from the deep, radiative interior is being transferred to the convective surface layers. This surface entropy rise is responsible for the swelling of the 2 $M_\odot$ star.

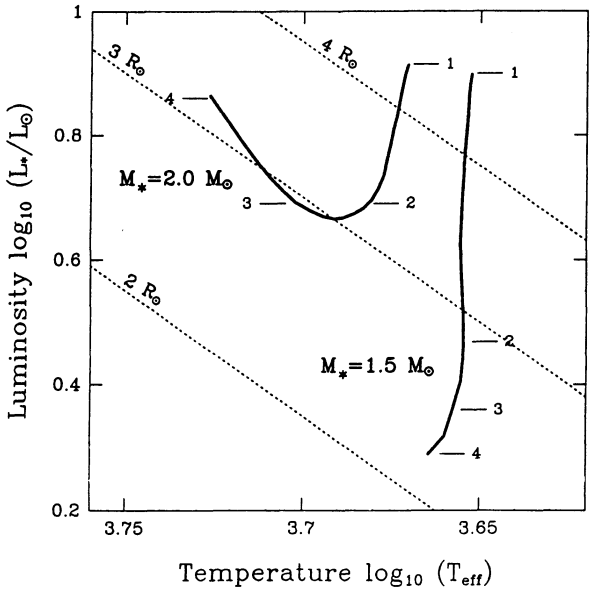

FIG. 4.—Early evolution in the H-R diagram of stars with $M_* = 1.5$ and 2.0 $M_\odot$. The labeled tick marks on each curve correspond to times of 0, 1, 2, and 3×10^6 yr after the end of protostellar accretion. The thin dashed lines are curves of constant radius.

The evolutionary trend seen in Figure 5 is identical, except for a shift in contraction ages, to that found in traditional calculations (e.g., Iben 1965). In particular, the entropy distribution is undisturbed by the fusion of residual deuterium. As shown in Figure 3, the deuterium begins at such a low concentration that it is quickly consumed. Since the deuterium luminosity is initially close to the steady state value in equation (3), $\Delta t_{\rm D}$, the time for exhaustion of the fuel, is

$$\Delta t_{\rm D} = \frac{f_{\rm D}\,\Delta M_{\rm D}[\mathrm{D/H}]XQ}{m_{\rm H}\,L_{\rm D}} = \frac{f_{\rm D}\,\Delta M_{\rm D}}{\dot{M}}\,, \tag{7}$$

where $Q = 5.5$ MeV is the energy released per fusion reaction, $X = 0.70$ is the fractional hydrogen abundance, and $m_{\rm H}$ is the hydrogen atom mass. The second equality follows from the fact that $\delta = [\mathrm{D/H}]XQm_{\rm H}$. Since, in the fully convective case, $\Delta M_{\rm D} = M_*$, we can read off $f_{\rm D}$ from Figure 3 to conclude that $\Delta t_{\rm D} = 30$ yr for 1.5 $M_\odot$ and only 1 yr for 2.0 $M_\odot$. These exceedingly brief times serve to emphasize the point that pre–main-sequence convection in these stars is driven by surface cooling, rather than central heating.

The rapid disappearance of deuterium is reflected in the stars' interior luminosities (Fig. 6). During steady state burning, the luminosity rose rapidly from the center. Farther out, it peaked at slightly less than the value in equation (3) (15 $L_\odot$ at $\dot{M} = 1 \times 10^{-5}\ M_\odot\ \mathrm{yr}^{-1}$), and then declined, as the deuterium-generated energy was absorbed in overlying layers of gas. The behavior is found in Figure 6, but only for the initial profiles of the two stars. After the period $\Delta t_{\rm D}$, the luminosities arise from gravitational contraction alone and have a

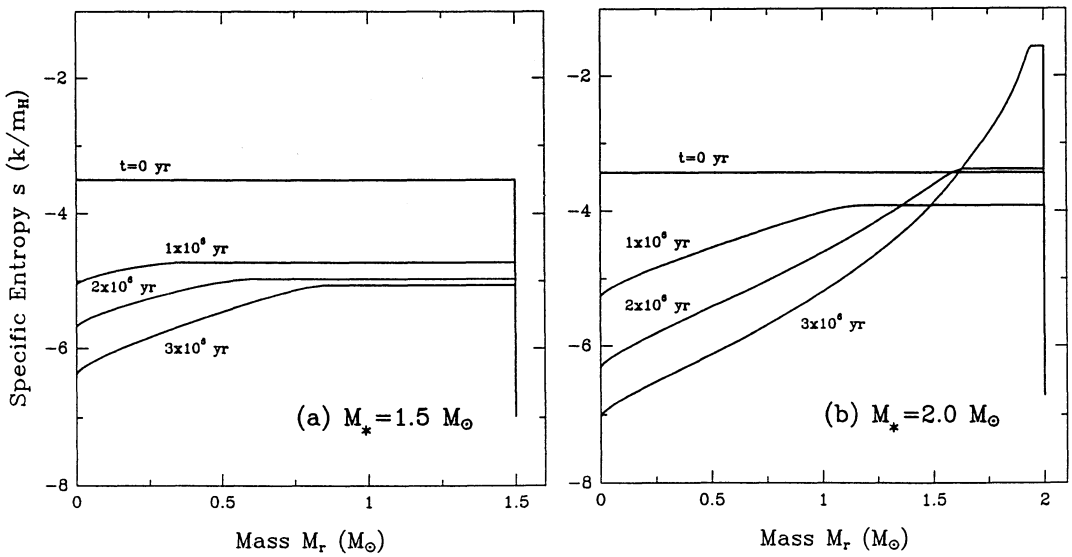

FIG. 5.—Early evolution of the entropy profile for (*a*) $M_* = 1.5\ M_\odot$ and (*b*) $M_* = 2.0\ M_\odot$. The curves show the specific entropy plotted as a function of internal mass coordinate. The very narrow surface radiative regions are not shown. Each curve is labeled by the corresponding evolutionary time. Specific entropy is measured in units of k_B/m_H, with the zero point arbitrarily set at $T = 2.05 \times 10^5$ K and $\rho = 5.16$ g cm^{-3}.

very different distribution. For the 1.5 $M_\odot$ star, most of whose interior is homologously contracting, the global loss of heat leads to a luminosity that monotonically rises toward the surface. For $M = 2.0\ M_\odot$, the absorption of heat by the convective layer causes the luminosity to fall in that region. Between $t = 1 \times 10^6$ yr and 3×10^6 yr, the surface luminosity rises despite the increase in stellar radius (see eq. [1]). This rise is linked, therefore, to the disappearance of the absorbing convective layer.

4.2. *Partially Convective Stars*

The most significant departure from classical pre–main-sequence evolution occurs for stars which have radiative central regions, but subsurface layers that are convective from the burning of residual deuterium. Referring once again to Figure 1, the relevant mass range is from M_2 to M_3, i.e., from 2.4 to 3.9 $M_\odot$ at $\dot{M} = 10^{-5}\ M_\odot$ yr^{-1}. Stars in this interval undergo thermal relaxation and nonhomologous contraction. The H-R diagram of Figure 7 shows the first 2×10^5 yr in the evolution of a 3.5 $M_\odot$ star. When the star is first optically visible, following the end of protostellar accretion, it is *underluminous*. That is, not only does the star skip entirely the traditional descent down a vertical Hayashi track, it actually appears below the bottom of this track. The reason is that the star's entropy distribution forces the surface temperature to the low values characteristic of fully convective stars, but its radius is much smaller than those of homologously contracting models (see § 2.3 of Stahler 1989). A small radius, by equation (2), implies a low luminosity, which can only increase through a redistribution of the internal entropy.

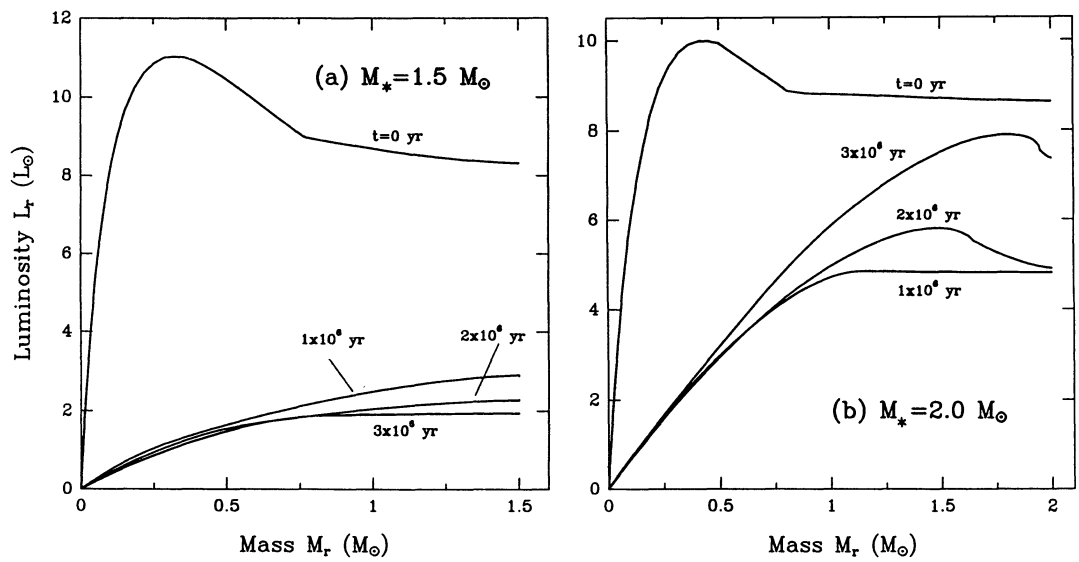

FIG. 6.—Early evolution of the luminosity profile for (*a*) $M_* = 1.5\ M_\odot$ and (*b*) $M_* = 2.0\ M_\odot$. As in Fig. 5, each curve is labeled by its evolutionary time. Notice how the internal luminosity *rises* in the more massive star.

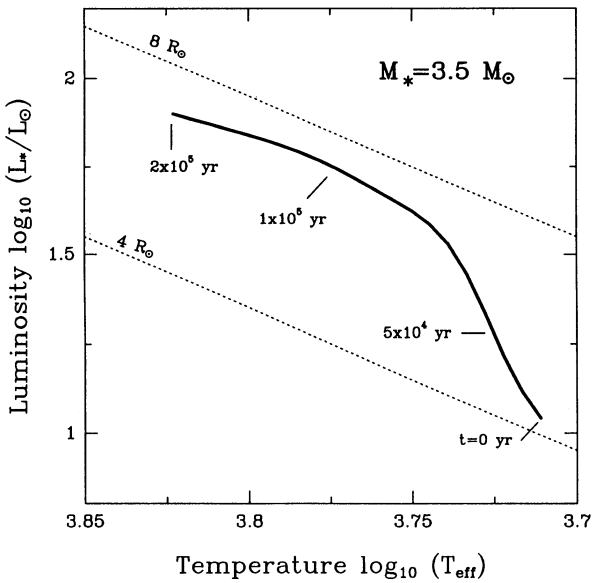

FIG. 7.—Early evolution in the H-R diagram of a 3.5 $M_\odot$ star. The thin dashed lines are curves of constant radius. Notice the swelling and brightening of the star during this period of thermal relaxation.

Figure 7 shows that the luminosity rise is accompanied by increases in both surface temperature and radius. The swelling is caused by heating the subsurface layers, just as in the 2 $M_\odot$ star. In a previous, simplified treatment of the relaxation process (Stahler 1989), the radius was artificially held constant, so that the luminosity rise depended solely on temperature. Since $T_{\rm eff}$ responds in a highly nonlinear fashion to heat input from the interior, the rise time for the luminosity was greatly underestimated. According to the present calculation, the surface luminosity in the 3.5 $M_\odot$ case increases for 1.2×10^5 yr before the radius reaches its maximum of 7.2 $R_\odot$. This point may conveniently be taken as the end of the thermal relaxation, since the star thereafter joins a conventional radiative track in the H-R diagram. The rise time is 10% of the total time of 1.2×10^6 yr for the star to contract to the ZAMS.[2]

The disappearance of internal convection during nonhomologous contraction can be seen in the evolution of specific entropy (Fig. 8*a*). At $t = 0$, the convection zone, in which the entropy is spatially constant, covers the outer 21% of the stellar mass. The central region soon contracts substantially, expelling heat to overlying layers. Thus, the central entropy declines while the outer entropy rises, swelling the star. Outer convection includes only 1% of the star's mass at $t = 7 \times 10^4$ yr; by this point, deuterium burning has also died out. At the time shown in the figure, 2×10^5 yr, the outer entropy has risen to a tall spike, and convection is confined to a thin region associated with hydrogen and helium ionization.

Figure 8*b* follows the relaxation of the internal luminosity. The maximum in L_r is at first located deep within the star, at $M_r = 1.9\ M_\odot$. Matter inside this point is losing heat, while exterior mass shells are gaining it. The position of the luminosity maximum migrates to the surface as the entropy is redistributed. By $t = 1.7 \times 10^5$ yr, the peak is located at the stellar surface, and L_* has increased by a factor of 6.5.

4.3. *Fully Radiative Stars*

During the protostar phase, thermal relaxation is marked by dramatic swelling of the star, and by retreat of convection toward the surface. Protostars which continue to accrete cloud matter after this time are fully radiative, and begin to contract under their own gravity, as seen in Figure 2. Pre–main-sequence stars descended from such protostars are therefore also fully radiative and thermally relaxed. In the H-R diagram, they appear immediately on the radiative portion of the appropriate classical evolutionary track. At a mass accretion rate of $10^{-5}\ M_\odot\ {\rm yr}^{-1}$, the stars that evolve in this fashion cover the interval in mass from 3.9 to 8.0 $M_\odot$. In stars more massive than the upper limit, ordinary hydrogen ignites during protostellar

[2] In this study, the ZAMS is defined as the point of equilibration of the main reaction network, which, for $M_* = 3.5\ M_\odot$, is the CN cycle; see Clayton 1983, chap. 5.

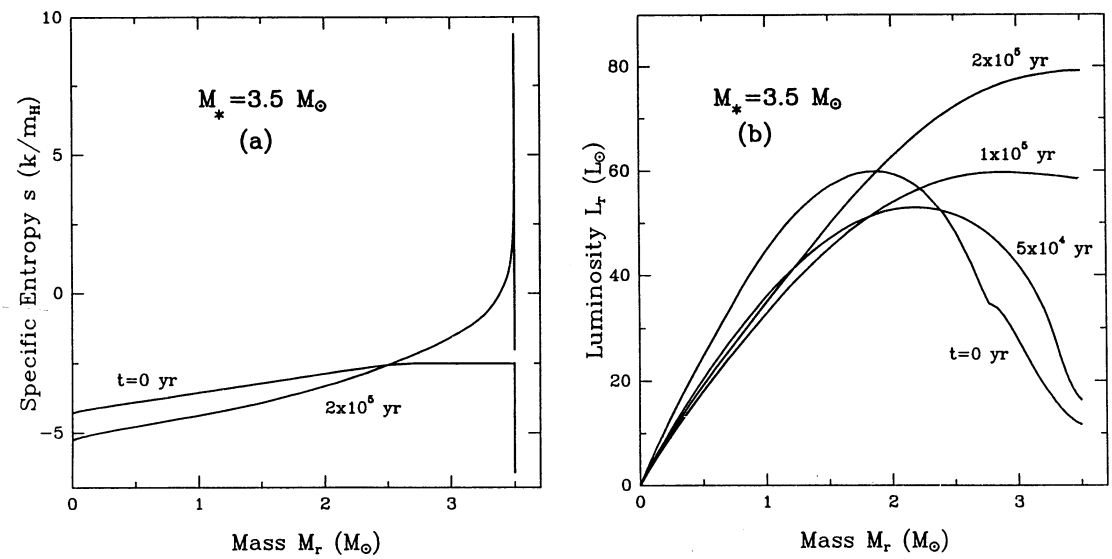

FIG. 8.—Thermal relaxation of a 3.5 $M_\odot$ star, showing the evolution of (*a*) the entropy profile and (*b*) the internal luminosity during the first 2×10^5 yr. As the specific entropy rises in the outer layers, the peak in luminosity also moves toward the surface. Both effects stem from the star's nonhomologous contraction.

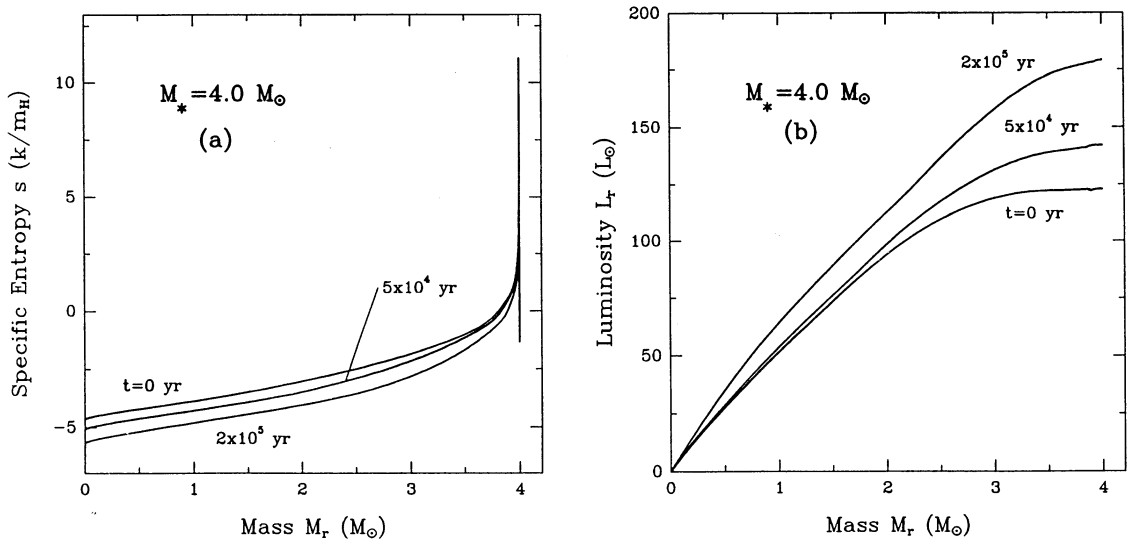

FIG. 9.—Early evolution of (*a*) the entropy profile and (*b*) the internal luminosity of a 4.0 $M_\odot$ star. Since the star is fully radiative, and therefore contracting homologously, there is a global drop in specific entropy and a corresponding rise in the internal luminosity.

accretion. Such stars exhibit no pre–main-sequence phase at all; once optically visible, they appear directly on the ZAMS.

Figure 9 depicts the evolution of the distribution of entropy and internal luminosity in a 4 $M_\odot$ star. The figure covers the first 2×10^5 yr of pre–main-sequence evolution, about one-seventh of the total contraction time to the ZAMS. The specific entropy (Fig. 9*a*) is now decreasing with time in all interior mass shells, a sign of homologous contraction. At any one time, the interior is radiative, i.e., the entropy is increasing outward, except for a very thin surface layer.

The distribution of luminosity (Fig. 9*b*) also shows no signs of the internal maxima characteristic of unrelaxed stars. As the star contracts, the average interior luminosity must rise as $R_*^{-1/2}$, according to equation (1). Such a rise is evident in the figure, which covers a period during which R_* drops by 18% from its initial value. During this same period, deuterium is burning in a radiative mantle covering the outer 10% of the stellar mass. The deuterium luminosity of 0.6 $L_\odot$, is, by now, a minor fraction of the surface luminosity L_*, which stems almost entirely from the bulk gravitational contraction of the star.

5. APPROACH TO THE MAIN SEQUENCE

5.1. *Evolution in the H-R Diagram*

Once each star has completed its thermal readjustment following accretion, it continues to contract until ordinary hydrogen ignites at its center. Figure 10 depicts the evolution of all our computed masses in the H-R diagram. The figure also includes results for 0.6 and 1.0 $M_\odot$ models (Parigi 1992), as examples of lower mass stars that remain convective for a longer portion of their pre–main-sequence lifetimes. All evolutionary tracks begin at the birthline (*dotted curve*) and end at the ZAMS; the latter has been omitted from the figure for clarity.

In comparison with previous calculations (Iben 1965; Ezer & Cameron 1967), our tracks occupy a much reduced portion of the diagram. This reduction is a consequence of our initial conditions, specifically, the modest radii attained by each star during its accretion period. For intermediate-mass stars, as for their lower mass counterparts, the starting luminosities are therefore much lower than previously envisioned. In addition, however, the surface temperatures of these stars begin *higher*. For example, a 5 $M_\odot$ star starts with $T_{\rm eff} = 1.2 \times 10^4$ K, in contrast to the value of 4400 K obtained by Iben (1965). The difference is that, in our calculation, the star has had time to relax thermally by radiative diffusion as a protostar. Its outermost layers become fully ionized, and the dominant opacity source in this region is no longer the H^- ion. Consequently, the pre–main-sequence surface temperature is no longer locked

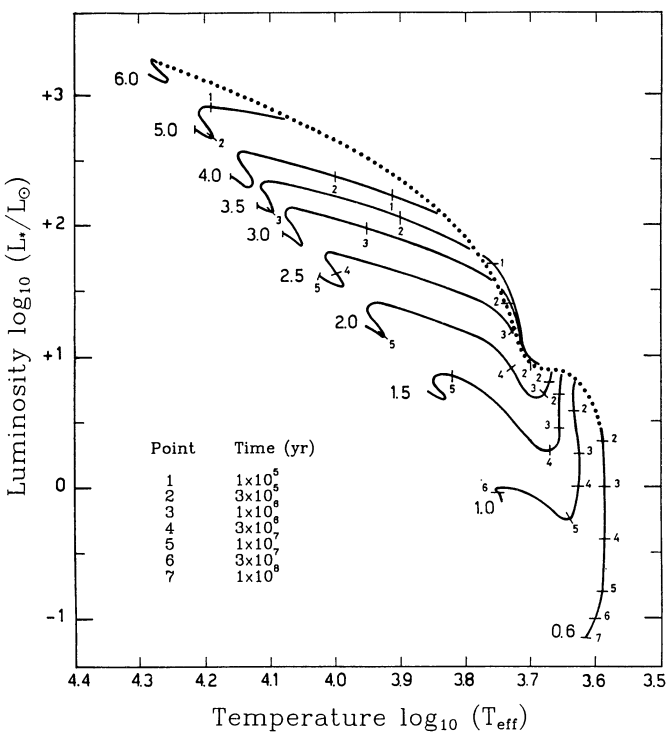

FIG. 10.—Evolutionary tracks in the H-R diagram for all computed masses. We also include the tracks for $M_* = 0.6$ $M_\odot$ and 1.0 $M_\odot$, as obtained by Parigi (1992). Each track is labeled by the corresponding mass in solar units. Tick marks indicate evolutionary times, as given in the table. Each track starts at the birthline (*dotted curve*) and ends at the ZAMS. The latter curve has been omitted for clarity.

TABLE 1

EVOLUTIONARY PROPERTIES

Property	1.0 $M_\odot$	1.5 $M_\odot$	2.0 $M_\odot$	2.5 $M_\odot$	3.0 $M_\odot$	3.5 $M_\odot$	4.0 $M_\odot$	5.0 $M_\odot$	6.0 $M_\odot$
					Initial				
R_* ($R_\odot$)	4.99	4.97	4.41	4.06	3.98	4.23	7.82	6.40	3.79
ΔM_{con} ($M_\odot$)	1.00	1.50	2.00	1.76	1.10	0.72	...	...	...
T_{eff} (K)	4.24×10^3	4.48×10^3	4.66×10^3	4.84×10^3	4.99×10^3	5.14×10^3	6.92×10^3	1.17×10^4	1.87×10^4
T_c (K)	1.64×10^6	2.51×10^6	3.47×10^6	4.66×10^6	5.54×10^6	6.42×10^6	7.30×10^6	1.27×10^7	2.46×10^7
					ZAMS				
R_* ($R_\odot$)	1.00	1.71	1.77	2.05	2.29	2.49	2.72	3.09	3.30
ΔM_{con} ($M_\odot$)	0.04	0.19	0.28	0.49	0.59	0.72	0.85	1.04	1.26
T_{eff} (K)	5.61×10^3	7.20×10^3	8.91×10^3	1.05×10^4	1.20×10^4	1.31×10^4	1.44×10^4	1.64×10^4	1.92×10^4
T_c (K)	1.20×10^7	1.57×10^7	1.84×10^7	1.92×10^7	2.00×10^7	2.10×10^7	2.15×10^7	2.25×10^7	2.50×10^7
					Timescales				
t_{rad} (yr)	...	9.43×10^6	3.36×10^6	1.30×10^6	4.23×10^5	7.39×10^4	...	...	...
t_{max} (yr)	2.75×10^7	1.01×10^7	5.38×10^6	2.66×10^6	1.35×10^6	7.38×10^5	4.15×10^5	1.02×10^5	...
t_{min} (yr)	...	1.10×10^7	6.33×10^6	3.18×10^6	1.76×10^6	9.93×10^5	5.77×10^5	1.75×10^5	...
t_{ZAMS} (yr)	3.16×10^7	1.20×10^7	8.35×10^6	3.90×10^6	2.02×10^6	1.25×10^6	8.16×10^5	2.32×10^5	4.00×10^4

to the relatively low values prescribed in the classical theory (Hayashi 1961).

Several key properties of our computed models, both at the beginning and end of their pre–main-sequence evolution, are given in Table 1. In addition to the stellar radius and the surface and central temperatures, the table also lists ΔM_{con}, the mass in the convection zone. For the ZAMS models, this convection is located at the center, and is driven by the strongly temperature-sensitive CN burning. Table 1 shows that, for $M_* \gtrsim 2\ M_\odot$, ΔM_{con} on the ZAMS comprises about 20% of the total stellar mass. This figure, as well as other model characteristics at late epochs, are in good agreement with the analogous results of Iben (1965) and Ezer & Cameron (1967).

Table 1 also lists several evolutionary times, all measured relative to the stars' appearance on the birthline.[3] The time t_{rad} marks the point at which the star becomes fully radiative; note that this event never occurs in the 1 $M_\odot$ case. Also given are t_{max} and t_{min}, which mark when the surface luminosity attains temporary maxima and minima prior to the ZAMS (see Fig. 10). The total duration times of the pre–main-sequence phase, listed in the table as t_{ZAMS}, are shorter than the corresponding values in Iben (1965), who continued his calculations beyond the equilibration point of ^{12}C. For most masses, the two estimates are within 30%, but the discrepancy is large for $M_* \gtrsim 4\ M_\odot$. Stars this massive begin, in our calculation, with radii only slightly larger than the ZAMS values. For $M_* = 8\ M_\odot$, the two radii coincide, and our value of t_{ZAMS} vanishes, as can be seen in Figure 10. In all evolutionary runs, we find that the release of energy through gravitational contraction contributes less than 3% of the total luminosity by the time the ZAMS is reached. We find no slowing of the contraction from deuterium burning, even for a mass as low as 1 $M_\odot$.

5.2. *Influence of Protostellar Accretion Rate*

We have previously explored the evolution of protostars accreting with an $\dot{M}$ as large as $10^{-4}\ M_\odot\ yr^{-1}$. In the H-R diagram, the resulting birthline sits rather high with respect to the observed upper envelope of Ae and Be stars (see Fig. 11 of Palla & Stahler 1992). Thus, we have maintained that an accretion rate of $10^{-5}\ M_\odot\ yr^{-1}$ is more appropriate. It remains true, however, that the physical conditions in clouds that produce intermediate-mass stars are poorly known. Hence, it is worthwhile to ask how pre–main-sequence evolution is altered when the progenitor stars are built up at a faster rate.

As before, we address this question through the behavior of several characteristic luminosities in the protostar phase. Figure 11 shows, in the same manner as Figure 1, the quantities L_{rad}, L_{surf}, L_{acc}, and L_D, now taken from the protostar sequence constructed with $\dot{M} = 10^{-4}\ M_\odot\ yr^{-1}$. Because protostars evolving at the higher rate have larger radii (see Fig. 2), each of the critical events described earlier is postponed to a larger mass. The values of M_1, M_2, and M_3 are now shifted to

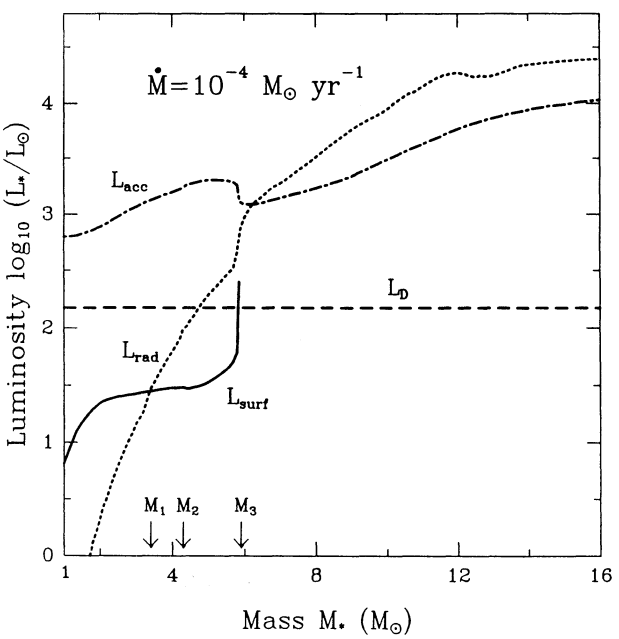

FIG. 11.—The mass dependence of luminosities in protostars accreting at $10^{-4}\ M_\odot\ yr^{-1}$; from Palla & Stahler (1992). Both luminosities and the three critical masses have the same meaning as in Fig. 1.

[3] Note that the times listed in Table 1 do not correspond to those in Fig. 10.

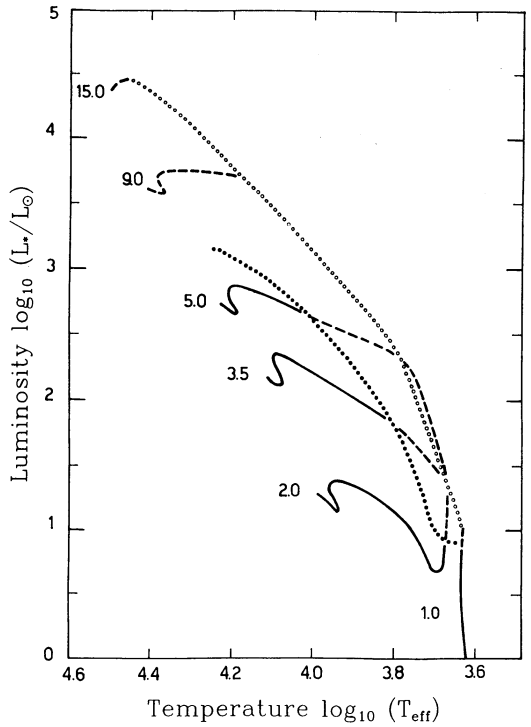

FIG. 12.—Effect of the protostellar mass accretion rate on pre–main-sequence evolution in the H-R diagram. The tracks of selected masses are shown schematically (*dashed curves*), starting from the birthline computed with $\dot{M} = 10^{-4}\ M_\odot\ \mathrm{yr}^{-1}$ (*open circles*). Stars of lower mass join onto standard tracks (*solid curves*) by the time they have crossed the birthline corresponding to $\dot{M} = 10^{-5}\ M_\odot\ \mathrm{yr}^{-1}$ (*dotted curve*). The displayed portions of the 9 and 15 $M_\odot$ tracks are from Iben (1965).

3.4, 4.3, and 5.9 $M_\odot$, respectively. Thus, the mass interval undergoing thermal relaxation is now 3.4 to 5.9 $M_\odot$. Because of the increased gap between M_1 and M_2, this group also includes stars which are fully convective as protostars, but have only a partially convective deuterium mantle within a time Δt_D after accretion ends. Furthermore, a visible pre–main-sequence phase is now possible for stars with masses as large as 15 $M_\odot$, the new point at which hydrogen ignites during accretion.

The higher accretion rate also means that the region of pre–main-sequence evolution in the H-R diagram is broadened, although this region is still much smaller than that envisioned in the classical theory. As seen in Figure 12, the new birthline (*open circles*), is shifted upward from the previous one (*dotted curve*), allowing tracks with larger mass to descend to the ZAMS, and extending those that were already present (*solid curves*) to include lower surface temperatures. Although the birthline positions of all masses have been marked accurately in the figure, the paths during thermal relaxation of the 3.5 and 5.0 $M_\odot$ stars are sketched only tentatively, since we have not followed these cases numerically. For both lower and higher masses, the tracks shown are still schematic, but there is less uncertainty, as the stars simply join onto the appropriate segments of their classical tracks. In particular, the 9 and 15 $M_\odot$ tracks shown here are adopted from Iben (1965).

6. DISCUSSION

In the classical theory of pre–main-sequence evolution, stars of every mass follow essentially the same behavior. Beginning as fully convective objects, they contract homologously until a central radiative core grows and, eventually, hydrogen ignites and stops further contraction. While this basic sequence of events still suffices for low-mass stars, we have shown how it must be substantially modified for more massive objects. The previous simple picture is now to be replaced by a more complex one. Some stars initially expand once they become optically visible, while others skip their early convective phase. Stars more massive than about 8 $M_\odot$ never have a pre–main-sequence phase at all and can only be observed as infrared, accreting protostars or as main-sequence or post–main-sequence objects.

We are encouraged that the present theory does seem to account for one basic property of intermediate-mass pre–main-sequence stars, their distribution in the H-R diagram. Figure 13 reproduces the theoretical tracks and birthline from Figure 10, together with observed luminosities and effective temperatures for a number of stars. The data for Herbig Ae and Be stars have been taken from Berrilli et al. (1992), while the observations of lower mass stars are from Strom et al. (1989). It is evident that the upper envelope of the stellar distribution is generally well matched by the theoretical birthline. Furthermore, this same upper envelope forms the locus of those stars with associated molecular outflows (Palla & Stahler 1990; Levreault 1988). Since the birthline was constructed using a protostellar mass accretion rate of $10^{-5}\ M_\odot\ \mathrm{yr}^{-1}$, we conclude that both low- and intermediate-mass stars could be formed in similar cloud environments (see also § 4 of Palla & Stahler 1992).

The H-R diagram of Figure 13 was constructed with the implicit assumption that most of the observed luminosity from any individual source indeed emanates from the central star.

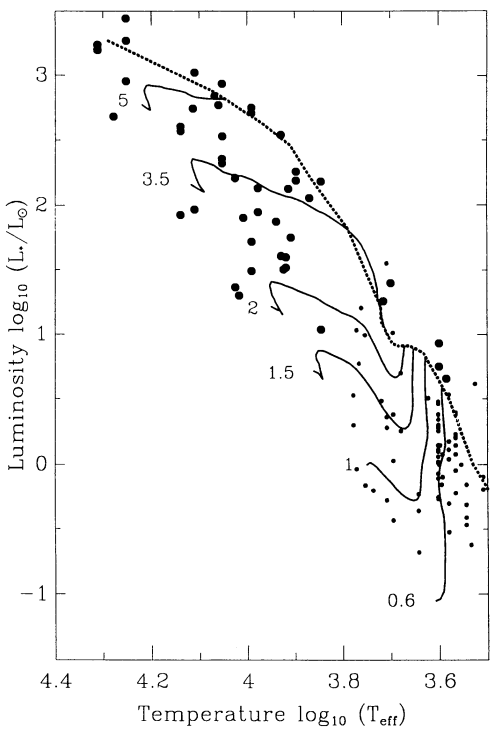

FIG. 13.—Observed distribution of low- and intermediate-mass pre–main-sequence stars in the H-R diagram. Data for Herbig Ae/Be stars (*large filled circles*) are taken from Berrilli et al. (1992), while the T Tauri stars (*small dots*) are from Strom et al. (1989). The theoretical tracks and birthline are the same as in Fig. 10.

Recently, this assumption has been disputed by Hillenbrand et al. (1992), who have advocated disk accretion as a primary luminosity source. These authors used multiwavelength observations to construct spectral energy distributions for 47 Ae and Be stars. For most of their sample (the "Group I" stars), Hillenbrand et al. have modeled the large infrared excesses with optically thick accretion disks containing central "holes." The holes, which typically extend to 10 stellar radii, are invoked to explain a characteristic dip in the spectral energy distributions between 1 and 2 μm (for a similar model, see Lada & Adams 1992). The derived mass flow rates through the disks, ranging from 10^{-6} to 10^{-4} $M_\odot$ yr^{-1}, are so high that the luminosity liberated through accretion is comparable to that attributed to the star itself. Consequently, once they have subtracted off the disk contributions to the luminosities, Hillenbrand et al. place their stars much lower in the H-R diagram than we have done in Figure 13.

For both low- and intermediate-mass stars, it is generally believed that the infrared excesses represent emission from heated dust. In our opinion, the disposition of this dust, and hence the underlying physical model, remains unclear, particularly for more luminous sources. Traditionally, the main argument for disks, invoked again by Hillenbrand et al., has been that a more isotropic distribution of dust would have obscured the visible radiation that is actually seen. Consider now a hypothetical pre–main-sequence star whose luminosity from disk accretion is comparable to that from bulk gravitational contraction. For such a star, we have

$$\frac{GM_* \dot{M}_d}{R_*} \approx L_* , \tag{8}$$

where $\dot{M}_d$ is the mass flow rate from the disk to the stellar surface.[4] Now M_* always exceeds the disk mass, M_d. Hence, the above relation implies

$$\frac{M_d}{\dot{M}_d} < \frac{GM_*^2}{R_* L_*} . \tag{9}$$

In other words, the time for the disk to be depleted is less than the characteristic evolutionary time of the central star. Over the life of the star, the disk must continually be replenished, presumably by matter from a more extended, infalling envelope. We are thus led back to the very difficulty which motivated the accretion disk hypothesis in the first place.

The problem can be mitigated by reducing the contribution of the disk, or other nonstellar component, to the total luminosity. Hillenbrand et al. assigned the central star a *main-sequence* spectral energy distribution, normalized to the observed, dereddened V magnitude. The remainder of the luminosity was assumed to arise from the disk. Since our own study has emphasized the extreme youth of Herbig Ae and Be stars, we question this procedure on general grounds. Moreover, it leads to the paradoxical result that those stars which have the greatest infrared excesses, and are therefore presumably the youngest, are placed closest to the main sequence in the H-R diagram (see Fig. 13 of Hillenbrand et al. 1992).

[4] Even if inner holes are present, disk material must ultimately reach the star, so R_* is the proper radius to use in eq. (8). Hillenbrand et al. effectively used the larger radius of the inner disk edge. Thus, their models do not account for the full accretion luminosity; see Hartmann, Kenyon, & Calvet (1993).

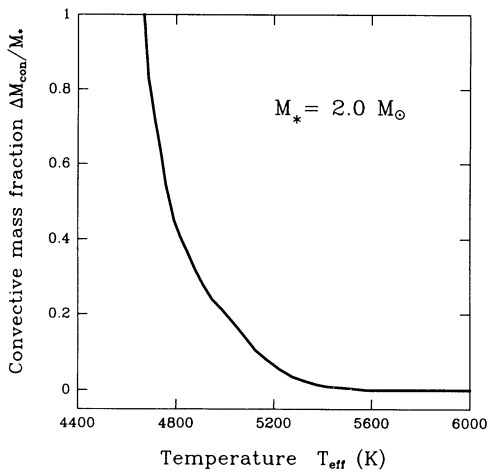

FIG. 14.—Retreat of convection in a 2.0 $M_\odot$ star. Shown as a function of effective temperature is ΔM_{con}, the mass in the convection zone, expressed here as a fraction of the stellar mass M_*.

Just as the infrared excesses in Ae and Be stars remain puzzling, so do their observed manifestations of surface activity, such as the P Cygni profiles frequently seen in Hα and other emission lines (Catala 1989). Earlier, we had speculated that subsurface burning of deuterium could maintain an outer convection zone which would, in turn, drive the surface activity (Palla & Stahler 1990). According to our present results, the retreat of outer convection *does* last a substantial fraction of a star's pre–main-sequence lifetime (see Fig. 5). During this retreat, however, the effective temperature remains relatively low, so that the star would not be observed with an A or B spectral type. Figure 14, in which we plot the mass of the convection zone, ΔM_{con}, against the surface temperature, illustrates this point in the case of a 2.0 $M_\odot$ star.

In retrospect, the fact that surface activity may *not* be associated with outer convection should hardly be surprising, if we consider the situation for low-mass stars. In the well-studied Taurus-Auriga cloud complex, roughly half the association members, the "naked" or "weak-lined" stars, do not exhibit such classical T Tauri attributes as emission lines or strong winds (Walter et al. 1988). And yet many of these same stars, like their classical counterparts, lie close to the birthline in the H-R diagram, and thus should have fully convective interiors (Stahler & Walter 1993). For young stars over a broad mass spectrum, therefore, surface activity seems to be unrelated to the presence or absence of outer convection. At this juncture, the clear observational delineation of a possible "naked" analog to Herbig Ae and Be stars would be extremely useful (see André et al. 1992 for one candidate source). If such a class could indeed be established, its morphology would provide important clues for a future, more complete theoretical treatment.

We thank Martin Cohen, Antonella Natta, and Steve Strom for useful discussions concerning the observational aspects of this problem. S. W. S. was supported principally by NSF grant AST 92-96096, and F. P. by ASI grant 91-RS-89. Much of the project was completed at Arcetri Observatory, where S. W. S. held a visiting professor position for 7 months in 1991. He is grateful to Franco Pacini for his hospitality and financial support.

REFERENCES

André, P., Deeny, B. D., Phillips, R. B., & Lestrade, J. F. 1992, ApJ, 401, 667
Baker, R. N., & Temesvary, S. 1966, Tables of Convective Stellar Envelopes (New York: Goddard Institute for Space Studies)
Berrilli, F., Corciulo, G., Ingrosso, G., Lorenzetti, D., Nisini, B., & Strafella, F. 1992, ApJ, 398, 254
Bodenheimer, P. 1965, ApJ, 142, 451
———. 1966, ApJ, 144, 709
Catala, C. 1989, in Low-Mass Star Formation and Pre–Main-Sequence Objects (ESO Conference and Workshop), ed. B. Reipurth (Munich: ESO), 471
Clayton, D. D. 1983, Principles of Stellar Evolution and Nucleosynthesis (New York: Gordon & Breach)
Cohen, M., & Kuhi, L. V. 1979, ApJS, 41, 743
Cox, J. P., & Giuli, R. T. 1968, Principles of Stellar Structure (New York: Gordon & Breach)
D'Antona, F. 1991, Mem. Soc. Astron. Ital., 62, 165
D'Antona, F., & Mazzitelli, I. 1984, A&A, 138, 431
Ezer, D., & Cameron, A. G. W. 1967, Canadian J. Phys., 45, 3429
Finkenzeller, U., & Jankovisc, I. 1984, A&AS, 57, 285
Finkenzeller, U., & Mundt, R. 1984, A&AS, 55, 109
Firnett, A. J., & Troesch, B. A. 1974, in Lecture Notes in Mathematics, 362, The Numerical Solution of Ordinary Differential Equations, ed. A. Dold & B. Eckman (New York: Springer-Verlag), 408
Fowler, W. A., Caughlan, G. R., & Zimmermann, B. A. 1975, ARA&A, 13, 69
Geiss, J., & Reeves, H. 1981, A&A, 93, 189
Grossman, A. N., & Graboske, H. C. 1971, ApJ, 164, 475
Harris, M. J., Fowler, W. A., Caughlan, G. R., & Zimmermann, B. A. 1983, ARA&A, 21, 165
Hartman, L., Kenyon, S. J., & Calvet, N. 1993, ApJ, 407, 219
Hayashi, C. 1961, PASJ, 13, 450
Henyey, L. G., LeLevier, R., & Levee, R. D. 1955, PASP, 67, 154
Herbig, G. H. 1960, ApJS, 4, 337
Hillenbrand, L. A., Strom, S. E., Vrba, F. J., & Keene, J. 1992, ApJ, 397, 613
Iben, I. 1965, ApJ, 141, 993
Lada, C., & Adams, F. C. 1992, ApJ, 393, 278
Larson, R. B. 1969, MNRAS, 145, 271
Levreault, R. M. 1988, ApJ, 330 897
Mazzitelli, I. 1989, in Low-Mass Star Formation and Pre–Main-Sequence Objects (ESO Conference and Workshop), ed. B. Reipurth (Munich: ESO), 433
Mazzitelli, I., & Moretti, M. 1980, ApJ, 235, 955
Natta, A., Palla, F., Butner, H. M., Evans, N. J., & Harvey, P. M. 1992, ApJ, 391, 805
Palla, F., & Stahler, S. W. 1990, ApJ, 360, L47
———. 1991, ApJ, 375, 288
———. 1992, ApJ, 392, 667
Parigi, G. 1992, thesis, Univ. of Florence
Salpeter, E. E. 1954, Mem. Soc. R. Sci. Liège, 14, 116
Shu, F. H. 1977, ApJ, 214, 488
Stahler, S. W. 1983, ApJ, 274, 822
———. 1988, ApJ, 332, 804
———. 1989, ApJ, 347, 950
Stahler, S. W., Palla, F., & Salpeter, E. E. 1986, ApJ, 302, 590
Stahler, S. W., Shu, F. H., & Taam, R. E. 1980, ApJ, 241, 637
Stahler, S. W., & Walter, F. M. 1993, in Protostars and Planets III, ed. E. H. Levy & J. Lunine (Tucson: Univ. of Arizona), 405
Strom, K. M., Strom, S. E., Edwards, S., Cabrit, S., & Skrutskie, M. F. 1989, AJ, 97, 1451
Strom, S. E., Strom, K. M., Yost, J., Carrasco, L., & Grasdalen, G. 1972, ApJ, 173, 353
Tijn A Djie, H. R. E., Remijn, L., & Thé, P. S. 1984, A&A, 134, 273
von Sengbusch, K. 1968, Zs. Ap., 69, 79
Walter, F., Brown, A., Mathieu, R. D., Myers, P. C., & Vrba, F. J. 1988, AJ, 96, 297
Winkler, K.-H., & Newman, M. J. 1980, ApJ, 236, 201